Accepted Manuscript

Electrochemical sensor for arsenite detection using graphene oxide assisted generation of prussian blue nanoparticles as enhanced signal label

Shao-Hua Wen, Yi Wang, Yan-Hong Yuan, Ru-Ping Liang, Jian-Ding Qiu

PII: S0003-2670(17)31335-1

DOI: 10.1016/j.aca.2017.11.057

Reference: ACA 235571

To appear in: *Analytica Chimica Acta*

Received Date: 3 September 2017

Revised Date: 10 November 2017

Accepted Date: 21 November 2017

Please cite this article as: S.-H. Wen, Y. Wang, Y.-H. Yuan, R.-P. Liang, J.-D. Qiu, Electrochemical sensor for arsenite detection using graphene oxide assisted generation of prussian blue nanoparticles as enhanced signal label, *Analytica Chimica Acta* (2017), doi: 10.1016/j.aca.2017.11.057.

GRAPHICAL ABSTRACT

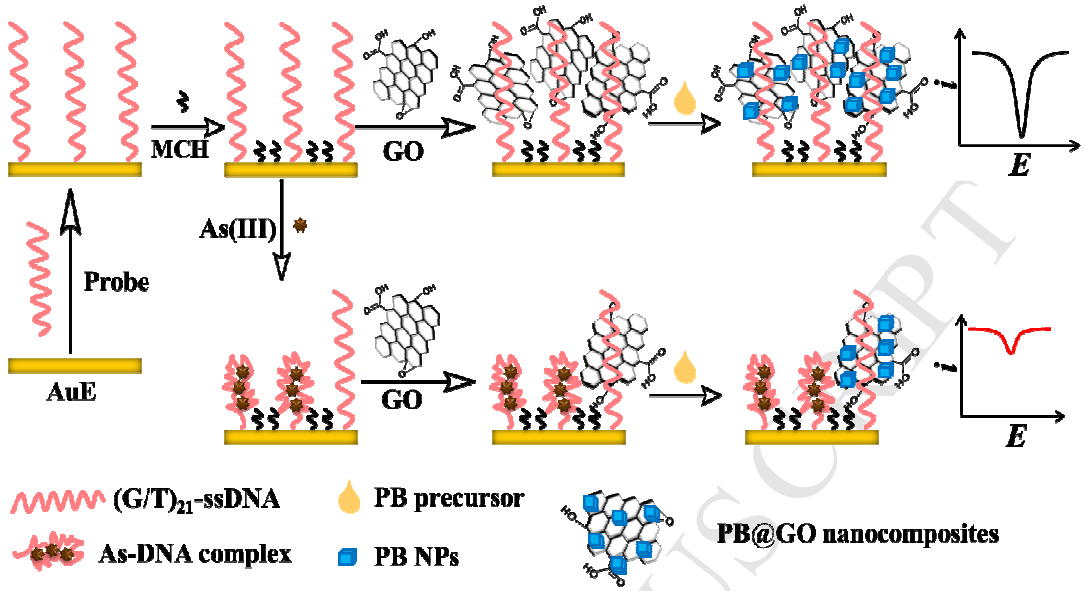

Schematic illustration of the sensor fabrication process and the generation of prussian blue nanoparticles on graphene oxide sheets used as electrochemical signal label for As(III) detection.

Electrochemical sensor for arsenite detection using graphene oxide assisted generation of prussian blue nanoparticles as enhanced signal label

Shao-Hua Wen, Yi Wang, Yan-Hong Yuan, Ru-Ping Liang, Jian-Ding Qiu*

College of Chemistry and Institute for Advanced Study, Nanchang University, Nanchang 330031, China

*Corresponding authors. Tel/Fax: +86-791-83969518. E-mail: jdqiu@ncu.edu.cn (J.D. Qiu).

ABSTRACT

An electrochemical sensor was fabricated for arsenite detection using graphene oxide-assisted generation of prussian blue nanoparticles as enhanced redox signal label. The 5′-thiolate-labeled $(GT)_{21}$-ssDNA was first self-assembled on a gold electrode surface via Au-S bond. Graphene oxide can interact with ssDNA through π-π stacking interaction and facilitate the generation of prussian blue nanoparticles on its surface as an electrochemically active indicator. In the absence of arsenite, plenty of graphene oxide/prussian blue nanoparticles can be adsorbed on the electrode surface to produce a stronger redox signal of prussian blue nanoparticles. While in the presence of arsenite, $(GT)_{21}$-ssDNA can recognize and combine with arsenite via hydrogen bonds to form $(GT)_{21}$-ssDNA/arsenite complex with a frizzy structure. The conformational change of $(GT)_{21}$-ssDNA led to less adsorption of graphene oxide/prussian blue nanoparticles on the electrode surface, resulting in a reduced redox response. The arsenite-induced $(GT)_{21}$-ssDNA structure switching can be used for sensitive detection of arsenite with a linear range from 0.2 to 500 ppb and a detection limit down to 0.058 ppb. Benefiting from $(GT)_{21}$-ssDNA containing arsenite recognition sequence, the proposed sensor exhibited excellent specificity against other heavy metal ions. The applicability of the electrochemical biosensor for arsenite assay in real water samples demonstrated the great potential of this strategy for trace arsenite detection in environment.

Keywords: Arsenite; ssDNA; Conformational change; Prussian blue; Graphene oxide; Electrochemical sensor.

1. Introduction

Arsenic (As), a ubiquitous trace element in the global environment, is mostly found in two inorganic forms, namely, arsenite (As(III)) and arsenate (As(V)). However, As(III) is more toxic, soluble, and mobile than As(V) [1]. Many studies have showed increased skin, lung and kidney cancer risk and other adverse health effects related to the brain, nervous system and digestive system for people chronic exposed to arsenic [2]. Therefore, elemental arsenic and many of its compounds have been classified as Group 1 carcinogens by the International Agency for Research on Cancer [3]. Recently, arsenic contaminated groundwater has become a serious and urgent environmental problem in many regions like South and Southeast Asia [4] and China [5], where millions and billions of people have been exposed to drinking water with arsenic contamination levels higher than the World Health Organization's (WHO) threshold value of 10 ppb (0.01 mg/L) [6].

Currently, various methods have been developed to detect heavy metal ions [7-13]. Particularly, technologies such as inductively coupled plasma mass spectrometry (ICP-MS) [14], hydride generation ICP-MS (HG-ICP-MS) [15], high performance liquid chromatography (HPLC-ICP-MS) [16], laser-induced desorption/ionization mass spectrometry (LDI-MS) [17] and surface-enhanced Raman scattering (SERS) [18] have been used for As(III) detection at low abundance. However, these techniques need cumbersome equipment, complex sample handling, long analysis time and even high cost [19,20]. Besides, these methods are neither capable of on-site field detection nor readily available in developing countries [20]. Therefore, it is

highly essential and significant to develop high-sensitive, low-cost and on-site field methods for the determination of trace As(III) in the groundwater.

Aptamers are DNA sequences with long-term stability, high affinity and selectivity for various targets like proteins, small molecules or ions. And aptamer-based biosensors have attracted extensive interests to detect trace amounts of different types of targets [21]. Based on aptamer or specific G-/T-rich ssDNA for the recognition of arsenite by strong hydrogen bonds, some sensors using different nanomaterials including carbon nanotubes [22], gold nanoparticles [23,24], silica nanoparticles [25], and quantum dots [26] for arsenite detection have made some progress in sensitivity and selectivity. Recently, DNA-based electrochemical sensors utilizing carbon nanotubes [27] or gold nanoparticles [28] have been reported for arsenite detection with high sensitivity. Graphene oxide (GO) has been used to design various sensors based on DNA recognition units and π−π stacking between nucleotide bases of ssDNA and carbon plane of GO [29]. Due to the abundant oxygen-containing functional groups, large specific surface area and good water solubility, GO has also been utilized as excellent platform to improve the analytical performance of biosensors by increasing loading of probes [30].

Prussian blue nanoparticles (PB NPs) have sparked intensive research interests in various fields due to its unique structure and superior properties [31]. Qiu et al. synthesized PB NPs-coated Au NPs by mixing Au NPs solution with the mixture solution of ferric(III) chloride and potassium ferricyanide under the acidic medium without any reductant [32], which provided a simple and convenient way to prepared

PB nanocomposites with hetero-structures and multiple-property. Recently, carbon nanotubes [33], carbon nanospheres [34], graphene [35] and GO [36,37] have been used for in-situ growth of PB NPs using the above similar principle to obtain various nanocomposites. Particularly, GO/PB and graphene/PB multi-functionalized nanocomposites have been synthesized using GO [36,37] or graphene [35] as supporting matrix and catalyst, which have been further employed as electrochemical label in electrochemical fields.

Herein, we have chosen GO as a supporting matrix that is beneficial to grow PB NPs, which can be used as an effective electrochemical label for As(III) sensing. The electrochemical biosensor is constructed by a 5′-thiolate-labeled ssDNA probe (containing the target As(III) recognition sequence) immobilized on the Au electrode surface via Au-S bonds. The generation of PB NPs on the GO sheets is subject to the target As(III)-regulated GO assembly with ssDNA. The recognition and interaction between ssDNA probe and As(III) can cause the subsequent less adsorption of GO with ssDNA probe because of As(III)-induced DNA conformational change, further resulting in less PB NPs generation on the GO sheets surface. As compared to the instance when As(III) is absent, a significant decrease in current signal is observed, which is dependent on the As(III) concentration. Therefore, such a sensor may be used as an effective candidate for detecting As(III) in environmental samples.

2. Experimental section

2.1. Reagents and chemicals

The thiol-modified 5′-SH-$(G/T)_{21}$-3′ ssDNA probe (sequence: 5’-SH-*GTG TGT*

GTG TGT GTG TGT GTG TGT GTG TGT GTG TGT GTG TGT-3'. The italicized letters represent the nucleotide sequences that can recognize and bind arsenite specifically) was purchased from Shanghai Sangon Biotechnology Co., Ltd (Shanghai, China). Graphite powder (99.8%, 325 mesh) was provided by Alfa Aesar. 6-Mercapto-1-hexanol (MCH, ≥97%) was purchased from Sigma-Aldrich (USA). Arsenite standard solution (As(III), 124.27 ppm) was purchased from National Sharing Platform for Reference Materials (Beijing, China). $FeCl_3 \cdot 6H_2O$ (99.0%), $K_3[Fe(CN)_6]$ (99.0%), ethylenediamine-N, N, N′, N′-tetraacetic acid disodium (EDTA), hydrogen peroxide (wt 30%), concentrated H_2SO_4 and HNO_3 were purchased from Sinopharm Chemical Reagents Co., Ltd (Shanghai, China). Prussian blue (PB) precursor solution was a mixture solution of 30 μM $FeCl_3$ and 30 μM $K_3[Fe(CN)_6]$, whose pH was adjusted to 5.0 by 0.1 M HCl aqueous solution. Phosphate buffer saline (PBS, 10 mM, pH 7.0) solution containing 0.1 M KCl was used as buffer solution. All the reagents were of analytical grade and were used without further purification. Ultrapure water (18.2 MΩ, Milli-Q Integral) was used in all experiments.

2.2. Instruments and characterization

Differential pulse voltammetry (DPV) and cyclic voltammetry (CV) experiments were performed with a CHI 630C workstation (Chenhua, Shanghai, China) by using a conventional three-electrode system with a gold electrode (AuE, Φ=2 mm) as the working electrode, a platinum wire as the auxiliary electrode and a saturated calomel reference electrode (SCE) as the reference electrode. Electrochemical impedance spectroscopy (EIS) was implemented on an Autolab PGSTAT30 electrochemical

workstation (Eco Chemie, Netherlands). Hitachi SU8010 scanning electron microscopy (SEM, Japan) was used to characterize the size and morphology of PB@GO nanocomposites. Transmission electron microscopy (TEM) images were obtained using a JEOL JEM-2010 transmission electron microscope (Japan) with an accelerating voltage of 200 kV. The UV–vis absorption spectra of GO and PB@GO nanocomposites were obtained with an UV-2450 ultraviolet-visible spectrophotometer (Shimadzu, Japan). Circular dichroism (CD) spectra of the $(GT)_{21}$-ssDNA probe and As(III) bound-DNA complex were collected with a Mos-450 Circular Dichroism Spectrometer (Bio-logic, France).

2.3. Fabrication of the electrochemical biosensor for As(III) determination

Graphene oxide (GO) was synthesized from natural graphite powder according to Hummer's method with a little modification [38]. Before modification with the $(GT)_{21}$-ssDNA probe, the gold electrode was chemically cleaned with a freshly prepared piranha solution, which is a 3:1 mixture of H_2SO_4 and H_2O_2, followed by repeatedly washing with ultrapure water. Afterwards, the electrode was consecutively polished with 1, 0.3, and 0.05 μm alumina slurry on a polishing pad and washed thoroughly with ultrapure water. Furthermore, the electrode was sequentially sonicated for 5 min in ultrapure water, absolute ethanol and ultrapure water before access to a mirror-like surface. Then the pretreated electrode was electrochemically cleaned in 0.5 M H_2SO_4 by potential scanning from –0.4 to +1.5 V until a reproducible cyclic voltammogram acquired. Finally, the electrode was washed with sufficient ultrapure water and blown dry with ultrapure nitrogen gas.

The cleaned electrode was first incubated with 60 μL 5′-SH-$(GT)_{21}$-ssDNA probe for 12 h at room temperature. Then, the ssDNA-modified electrode was subjected to stream rinsing and blocking the unspecific sites with 2.0 mM MCH for 2 h. After the electrode was incubated in As(III) solution for 3 h and thoroughly rinsing with ultrapure water, the electrode was immersed in 0.5 mg/mL GO solution for 1 h and subsequently incubated with PB precursor solution (30 μM $FeCl_3/K_3[Fe(CN)_6]$ with equal molar ratio, pH 5.0) for 30 min at room temperature. After rinsing with PBS buffer, PB NPs@GO nanocomposites were generated on the ssDNA-modified electrode surface as electrochemical mediator and used for the quantitative determination of As(III). Finally, the resulted PB NPs@GO/ssDNA modified electrode was washed with ultrapure water and stored at 4 ºC.

2.4. Electrochemical measurements

All electrochemical experiments were carried out in a conventional electrochemical cell containing a three-electrode arrangement. Cyclic voltammetry (CV) and electrochemical impendence spectra (EIS) measurements of the electrode fabrication were performed in a PBS buffer containing 5 mM $K_3[Fe(CN)_6]/K_4[Fe(CN)_6]$ (1:1). CVs were scanned from –0.4 V to +0.6 V at a scan rate of 100 mV/s. The impedance measurements were recorded at an alternating current voltage of 5 mV amplitude within the frequency range of 0.01 Hz to 100 kHz. The DPV measurement was used to measure the electrochemical signal of PB NPs in a PBS buffer and taken under the conditions: the potential range was from –0.3 to +0.4 V, modulation amplitude was 0.05 V, pulse width was 0.05 s, and sample width was 0.0167 s.

2.5. Real samples analysis

Three different real samples (tap water, Ganjiang Rriver water and Runxi Lake water) were used in this study. The river water and lake water samples were first centrifuged at 12 000 rpm for 10 min and filtered by a 0.22 μm membrane to detach the suspension and solid impurities. The pH of the sample solutions were then adjusted to 7.5. The solutions were next spiked with different concentrations (0.2 ppb, 10 ppb) of standard As(III) solution. The detection of As(III) in different samples was then performed using the proposed electrochemical biosensor and inductively coupled plasma mass spectrometry (ICP-MS).

3. Results and discussion

3.1. Sensing principle of the proposed sensor

As shown in Scheme 1, the sensing principle of the developed electrochemical biosensor is based on the generation of PB NPs as electrochemical label and GO as the supporting matrix for signal amplification. Firstly, the thiol-modified $(GT)_{21}$-ssDNA probe can be assembled on the Au electrode surface via the strong Au-S bond to obtain the As(III) recognition layer. Afterwards, the electrode surface is passivated with MCH to prevent the nonspecific adsorption. GO can interact with ssDNA through π-π stacking between nucleotide bases of single-stranded DNA and carbon plane of GO [29]. Moreover, GO can also be used as supporting matrix and assistant catalyst for facile generation of PB NPs via direct redox reaction among GO sheets, $[Fe(CN)_6]^{3-}$ and Fe^{3+} [34,35,39]. In the absence of As(III), plenty of GO sheets can be adsorbed on the ssDNA-modified electrode surface, providing a favorable

platform for the generation of abundant PB NPs on the GO sheets and thus produces a significant peak current of PB NPs. While in the presence of As(III), the $(GT)_{21}$-ssDNA probe can recognize and combine with As(III) by hydrogen bonds [22,23], inducing the conformational change of ssDNA probe and subsequently resulting in less adsorption of GO. Thus, few PB NPs generate on the ssDNA-modified electrode surface, producing a decreased redox peak current of PB NPs. The decrease extent of the peak current is dependent on the As(III) concentration. Therefore, by taking advantages of the generation of PB NPs on GO surface, the GO-assisted current signal amplification and As(III)-regulated GO assembly with ssDNA, the ultrasensitive detection of As(III) is easily realized using this electrochemical biosensor.

Scheme 1

3.2. CD characterization

Firstly, the interaction between As(III) and $(GT)_{21}$-ssDNA probe was investigated through circular dichroism technique, which is usually used to monitor the the confirmation of some biomolecules such as proteins and nucleic acids. Fig. 1 shows the CD spectra of the $(GT)_{21}$-ssDNA probe and ssDNA probe reacted with As(III). The ssDNA probe has a negative peak at ~262 nm and a positive peak at ~286 nm (curve a), which were in conformity with previous literatures [22,23]. After reacted with As(III), the values of both negative and positive peaks decreased significantly (curve b), which resulted from As(III) binding with some bases of the DNA probe and subsequently altering its conformation, consequently restrained the strong π-π^*

transition of bases with deoxyribose [23]. The CD spectra shows the evidence that As(III) can interact with $(GT)_{21}$-ssDNA probe and alter its conformation, which probably provided the basic feasibility rules of the proposed biosensor.

Fig. 1

3.3. Characterization of the PB@GO nanocomposites

The morphology of the electrode surface before and after assembly of PB NPs has been characterized by SEM (Fig. 2). The ssDNA/MCH/AuE surface is smooth (Fig. 2A). When GO/ssDNA/MCH/AuE was incubated with PB precursor solution, a mass of cube PB NPs with the average size of 32±10 nm were generated on the GO sheets (Fig. 2B). The morphology of the PB NPs generated on the GO/ssDNA/MCH/AuE is similar with that of the PB/GO nanocomposites synthesized by mixing PB precursor and GO solution under acidic condition (Fig. S1).

UV−vis absorption spectroscopy was first used to confirm the composition of PB@GO nanocomposites. As shown in Fig. S1A, the UV–vis spectrum of GO sheets (curve a) shows two characteristic absorption peaks at 230 and 300 nm respectively deriving from π-π* transition of the C=C band and n-π* transition of the C=O band, which were consistent with the previous report [40]. After formation of PB NPs@GO nanocomposites, a new absorption peak (curve b) was displayed at ~680 nm that should be attributed to PB nanoparticles in the nanocomposites [41]. The UV−vis absorption spectrum of PB NPs shows an obvious characteristic peak at approximately ~680 nm, which could be attributed to the intermetallic charge-transfer band from Fe^{2+} to Fe^{3+} in PB NPs [41]. From the inset of Fig. S1A, the color of the

PB@GO nanocomposites (tube 1) is cyan different from GO solution (tube 2). Therefore, the results indicated that the PB@GO nanocomposites were successfully synthesized by easily mixing and stirring the mixture of PB precursor and GO solution under acidic condition.

Fig. 2

3.4. Electrochemical characterization of the proposed biosensor

The stepwise fabrication process of the proposed biosensor was first characterized in PBS buffer containing 5 mM $[Fe(CN)_6]^{3-/4-}$ by CV and EIS, and the results were displayed in Fig. 3. As shown in Fig. 3A, a couple of well-defined redox peaks corresponding to the electrochemical process of $[Fe(CN)_6]^{3-/4-}$ couple is occurred on the bare AuE (curve a). When $(GT)_{21}$-ssDNA/MCH were modified on AuE surface, the oxidation peak currents obviously decreased from 46.52 μA (curve a) to 32.94 μA (curve b), which was inhibited by the negatively charged phosphate backbone of DNA probes and indicated that probes had been successfully anchored on the AuE surface. After the GO sheets were assembled on the ssDNA-modified AuE surface via π-π stacking interaction [29], the oxidation peak currents further reduced to 21.08 μA (curve c) due to the electrostatic repulsion between the negatively charged carboxyl groups of GO and $[Fe(CN)_6]^{3-/4-}$. However, when the DNA/MCH-AuE was treated with As(III) and then incubated with GO sheets, the oxidation peak currents would slightly increase to 27.31 μA (curve d), which suggested that As(III)-induced DNA conformational change could regulate the adsorption of GO sheets on the surface of DNA/MCH-AuE, and the Faradic electron transfer process was slightly enhanced by

the less adsorption of the negatively charged GO sheets.

In addition, EIS can provide sensitive information about the interface properties change of the Au electrode. In EIS spectrum, the differences in the electron transfer resistance (R_{et}) can be reflected on the semicircle diameter of the Nyquist plots: the increase of semicircle diameter in the high-frequency region can directly reflect the increase of the interfacial R_{et}. As depicted in Fig. 3B, compared with a very small semicircle domain with R_{et} (~502.9 Ω) of the bare AuE (curve a), an obviously increased R_{et} (~5175.8 Ω) is detected from $(GT)_{21}$-ssDNA/MCH/AuE (curve b), indicating that the coated layer of ssDNA/MCH on the electrode surface blocked the approaching of $[Fe(CN)_6]^{3-/4-}$ to electrode surface due to the electrostatic repulsion interaction. When GO sheets were further assembled onto the electrode interface, the R_{et} value further increased to 8804.5 Ω (curve c), which was caused by the negatively charged GO sheets assembled to electrode surface. After incubating $(GT)_{21}$-ssDNA/MCH/AuE with As(III) and then treated with GO solution, it was found the R_{et} value decreased significantly with the value of 6326.1 Ω, suggesting that As(III)-induced DNA conformational change could regulate the adsorption of GO sheets on the electrode surface and then accelerate the electron transfer of $[Fe(CN)_6]^{3-/4-}$ ions on the electrode interface (curve d). Therefore, from the results of both above CV and EIS experiments, it can be confirmed that the As(III)-regulated GO assembly-based with DNA probe functionalized electrode interface had been well fabricated as expected.

Fig. 3

The stepwise assembly occurring on the AuE surface was also confirmed by electrochemical measurements in PBS buffer. As shown in Fig. 4A, the CVs at AuE (curve a), $(GT)_{21}$-ssDNA/MCH/AuE (curve b) and GO/ssDNA/MCH/AuE (curve c) do not show any detectable redox peak current in PBS buffer. When the GO/ssDNA/MCH/AuE was treated with PB precursor solution, a pair of redox peaks corresponding to PB NPs were observed (curve d), suggested the successfully generation of PB NPs on GO sheets. As a control, the electrochemical response of ssDNA/MCH/AuE directly treated with PB precursor solution without GO modification was also investigated (curve e), and the redox peaks current of PB NPs at this electrode were obviously smaller than that on the GO/ssDNA/MCH/AuE (curve d). As shown in Fig. 4B, the anodic peak current of PB was -6.4 μA on ssDNA/MCH/AuE in the presence of GO (column d), which was eight times than that of -0.8 μA in the absence of GO (column e). These results suggested that the adsorbed GO on ssDNA/MCH/AuE played an important role to generate massive PB NPs and further enhance its current response due to its large surface area effect. Upon the As(III)-induced conformation change of the $(GT)_{21}$-ssDNA and the successful adsorption of GO onto the residuary ssDNA, the redox currents distinctly decreased caused by less PB NPs generated on the GO sheets surface (curve f and column f). The results indicated that the ssDNA probe reaction with As(III) led to the formation of DNA-As(III) frizzy structure, and less GO sheets can be absorbed on ssDNA-modified electrode surface by π-π stacking interaction, so the less PB NPs could generate on the GO sheets surface.

Fig. 4

3.5. Analytical performance of the electrochemical biosensor

Experimental conditions including the ssDNA probe concentration, the binding time between ssDNA and GO, the concentration of PB precursor solution, the generation time of PB/GO composite, the reaction pH and the incubation time of As(III) were optimized (Fig. S2), and the optimized experimental conditions (4.0 μM ssDNA, 30 μM PB precursor solution, 60 min for GO adsorption, 30 min for PB NPs generation, pH 7.5 for reaction system and the incubation time of 3.0 h for As(III) binding reaction) were chosen for the following experiments. The proposed electrochemical biosensor using GO sheets as the supporting matrix for the signal amplification strategy was challenged with different concentrations of As(III). The performance of the developed biosensor for the detecting of target As(III) was initially investigated in PBS buffer using DPV measurement. The current responses of the biosensor decreased along with the increase in As(III) concentration (Fig. 5A) owing to the hydrogen bonds interaction between G/T bases and target As(III) and the formation of As(III)-DNA frizzy structure. Moreover, as shown in inset of Fig. 5B, the calibration curve exhibits a linear relationship between the measured DPV peak currents and the logarithm values of the target As(III) concentrations within the range from 0.2 ppb to 500 ppb with the correlation equation of $I\ (\mu A) = 1.5156 \times \mathrm{Log}\ C_{As(III)} - 6.6241$ ($R^2 = 0.997$). The method detection limit (MDL) is calculated to be 0.058 ppb (S/N = 3), which is much lower than the WHO guideline of 10 ppb. The limit of quantification (LOQ, the lowest concentration at which the accuracy fell between

80% and 120% and the precision had a value of ≤10% under nine measurements) of the sensor was 0.020 ppb. The analytical performances of various biosensors were summarized in Table S1. The linear range and MDL of this biosensor were comparable to or even better than those of previously reported methods, due to the strong binding interaction between As(III) and G/T bases and As(III)-regulated GO sheets assembly with ssDNA for signal output. In particular, this electrochemical biosensor was better than those reported colorimetric and fluorescent methods due to the signal response amplification and sensitivity improvement of self-sensitive electrochemical techniques. Furthermore, the electrochemical biosensor used in this work was much simpler in operation and lower in cost compared with the bulky and expensive instruments.

The reproducibility of the proposed biosensor was evaluated by intra- and inter-assay coefficients of variation (CVs). The intra-assay precision of the analytical strategy was evaluated by analyzing one biosensor for five replicate determinations. The CVs of the intra-assay were 3.6% and 4.7% at 1 and 10 ppb As(III), respectively. Similarly, the inter-assay CVs on five biosensors were 4.2% and 5.6% at 1 and 10 ppb As(III), respectively. These results demonstrated acceptable reproducibility and precision of the proposed biosensor. In addition, the biosensor could be stored at 4 $^{\circ}$C. In this way, over 95% of the initial response remained after 1 week, indicating acceptable stability.

Fig. 5

3.6. Selectivity of the electrochemical biosensor.

To evaluate the specificity of the developed biosensor towards the target As(III), the response $(I_0-I)/I_0$ of the biosensor was tested in aqueous solutions containing variously common ions that may exist in lake water or underground water. As shown in Fig. 6, the biosensor exhibits good selectivity toward the target As(III) with other 15 interfering ions showing almost no response only except Hg^{2+} ions. A significant interference from Hg^{2+} may be attributed to the formation of self-folded structure of T-Hg-T structure between Hg^{2+} and (GT)-rich ssDNA probe [42]. So the selectivity of the assay toward As(III) ion was improved further by the addition of a chelating ligand EDTA [43]. Further investigation demonstrated that EDTA as an effective chelator can capture Hg^{2+} from the T-Hg-T complex, and thus the $(GT)_{21}$-ssDNA retained the random coil state. So EDTA had been chosen as the effective chelator for Hg^{2+} of water samples. Additionally, with the help of EDTA, no obvious variation in the peak currents were found in the samples containing those interfering ions other than As(III). The specificity for other interfering ions (except Hg^{2+}) may be ascribed to the strong affinity of the capture ssDNA probe to its target As(III) and the good adsorption ability between ssDNA and GO that was effectively regulated by As(III)-induced ssDNA conformational change. The mixture (Mix) (consisted of the 16 interference metal ions (100 ppb), 100 ppb As(III) and 10 μM EDTA) on the electrochemical biosensor was investigated, and it was clearly that $(I_0-I)/I_0$ was similar to the case of As(III) only existed. These results validated that the strategy can meet the selectivity requirements of the As(III) assay in environmental samples.

Fig. 6

3.7. Real sample analysis.

To further test the practicability of the developed biosensor toward its target As(III) in environmental samples, recovery experiments were carried out by spiking As(III) at different concentrations into three kinds of water samples (tap water, Ganjiang river and Runxi lake). It should be noted that Ganjiang river and Runxi lake samples were first treated with EDTA to eliminate the interference from Hg^{2+} and thus to obtain the accuracy of the electrochemical measurement. No As(III) was found in tap water and Ganjiang River water samples, indicated that the concentration of As(III) in tap water and Ganjiang River water samples was extremely low and not detectable. The concentration of As(III) in the original lake water sample was measured as 0.16 ppb. When different concentrations of standard As(III) solution were spiked into tap water, Ganjiang River water and Runxi Lake water samples, the relative recoveries were calculated to be 95%–106% and the RSDs were 3.6-5.1%. The results obtained by this method were comparable with those obtained by ICP-MS method (Table 1). The above results indicated that the developed electrochemical biosensor had good reliability and accuracy and can be successfully used for the determination of As(III) in environmental water samples.

Table 1

4. Conclusion

In this work, an ultra-sensitive electrochemical biosensor have been developed for the determination of As(III) by utilizing GO sheets as the supporting matrix for signal amplification and generation of PB NPs on the GO sheets as the electrochemical label.

Without any assistant reductant, PB@GO nanocomposites can be obtained only by adding GO solution to the mixture of ferric(III) chloride and potassium ferricyanide under acidic conditions. Such in-situ growth of PB NPs on the GO sheets have been used as electrochemical probes for the label-free detection of As(III). On the basis of the convenient and generation of PB nanoparticles on the GO sheets and the target As(III)-regulated GO assembly with ssDNA by As(III)-induced ssDNA conformational change, a sensitive biosensor has been presented with a broad detection range and low detection limit. Furthermore, the introduction of EDTA to the assay system can successfully eliminate the interference of Hg^{2+} ions, which allow the high-selective detection of As(III). The encouraging results obtained on real samples using this low-cost and label-free biosensor provide an alternative way for further applications such as the realization of analysis As(III) or other toxicants in complex environmental samples by simply replacing the specific aptamer.

Competing interests

The authors declare no competing financial interest.

Acknowledgments

This work is supported by the National Natural Science Foundation of China (21675078 and 21475056), the program for major academic and technical leaders of Jiangxi province (20123BCB22003 and 20162BCB22013) and the Key Project of Scientific and Technological Innovation Talents in Jiangxi Province (20165BCB18022).

Appendix A. Supplementary data

Supplementary data associated with this article can be found, in the online version, at http://dx.doi.org/XXXXX/.

References

[1] V.K. Sharma, M. Sohn, Aquatic arsenic: Toxicity, speciation, transformations, and remediation, Environ. Int.35 (2009) 743-759.

[2] K. Jomova, Z. Jenisova, M. Feszterova, S. Baros, J. Liska, D. Hudecova, C.J. Rhodes, M. Valko, Arsenic: toxicity, oxidative stress and human disease, J. Appl. Toxicol. 31 (2011) 95-107.

[3] IARC, Monographs on the evaluation of carcinogenic risks to humans, http://monographs.iarc.fr/ENG/Classification (accessed 2016).

[4] S. Fendorf, H.A. Michael, A. van Geen, Spatial and Temporal Variations of Groundwater Arsenic in South and Southeast Asia, Science 328 (2010) 1123-1127.

[5] L. Rodríguez-Lado, G. Sun, M. Berg, Q. Zhang, H. Xue, Q. Zheng, C.A. Johnson, Groundwater Arsenic Contamination Throughout China, Science 341 (2013) 866.

[6] WHO-Arsenic, http://www.who.int/mediacentre/factsheets/fs372/en/ (Updated 2016).

[7] M.K. Bojdi, M.H. Mashhadizadeh, M. Behbahani, A. Farahani, S.S.H. Davarani, A. Bagheri, Synthesis, characterization and application of novel lead imprinted polymer nanoparticles as a high selective electrochemical sensor for ultra-trace determination of lead ions in complex matrixes, Electrochim. Acta 136 (2014) 59-65.

[8] M.K. Bojdi, M. Behbahani, A. Sahragard, B.G. Amin, A. Fakhari, A. Bagheri, A palladium imprinted polymer for highly selective and sensitive electrochemical determination of ultra-trace of palladium ions, Electrochim. Acta 149 (2014) 108-116.

[9] M.K. Bojdi, M. Behbahani, M. Najafi, A. Bagheri, F. Omidi, S. Salimi, Selective and Sensitive Determination of Uranyl Ions in Complex Matrices by Ion Imprinted

Polymers-Based Electrochemical Sensor, Electroanal. 27 (2015) 2458-2467.

[10] M.K. Bojdi, M. Behbahani, F. Omidi, G. Hesam, Application of a novel electrochemical sensor based on modified siliceous mesocellular foam for electrochemical detection of ultra-trace amounts of mercury ions, New J. Chem. 40 (2016) 4519-4527.

[11] V. Zarezade, M. Behbahani, F. Omidi, H.S. Abandansari, G. Hesam, A new magnetic tailor made polymer for separation and trace determination of cadmium ions by flame atomic absorption spectrophotometry, RSC Adv. 6 (2016) 103499-103507.

[12] H.R. Sobhi, M. Ghambarian, A. Esrafili, M. Behbahani, A nanomagnetic and 3-mercaptopropyl-functionalized silica powder for dispersive solid phase extraction of Hg(II) prior to its determination by continuous-flow cold vapor AAS, Microchim.Acta 184 (2017) 2317-2323.

[13] H. Ebrahimzadeh, M. Behbahani, A novel lead imprinted polymer as the selective solid phase for extraction and trace detection of lead ions by flame atomic absorption spectrophotometry: Synthesis, characterization and analytical application, Arab. J. Chem. 10 (2017) S2499-S2508.

[14] E. Bolea-Fernandez, L. Balcaen, M. Resano, F. Vanhaecke, Interference-free determination of ultra-trace concentrations of arsenic and selenium using methyl fluoride as a reaction gas in ICP–MS/MS, Anal. Bioanal. Chem. 407 (2015) 919-929.

[15] L.W.L. Chen, X. Lu, X.C. Le, Complementary chromatography separation combined with hydride generation–inductively coupled plasma mass spectrometry for arsenic speciation in human urine, Anal. Chim. Acta 675 (2010) 71-75.

[16] W. Maher, S. Foster, F. Krikowa, E. Donner, E. Lombi, Measurement of Inorganic Arsenic Species in Rice after Nitric Acid Extraction by HPLC-ICPMS: Verification Using XANES, Environ.Sci. Technol. 47 (2013) 5821-5827.

[17] C.-I. Weng, J.-S. Cang, J.-Y. Chang, T.-M. Hsiung, B. Unnikrishnan, Y.-L. Hung, Y.-T. Tseng, Y.-J. Li, Y.-W. Shen, C.-C. Huang, Detection of Arsenic(III) through Pulsed Laser-Induced Desorption/Ionization of Gold Nanoparticles on Cellulose Membranes, Anal. Chem. 86 (2014) 3167-3173.

[18] M. Mulvihill, A. Tao, K. Benjauthrit, J. Arnold, P. Yang, Surface-Enhanced Raman Spectroscopy for Trace Arsenic Detection in Contaminated Water, Angew. Chem. Int. Ed. 47 (2008) 6456-6460.

[19] B. Sadee, M.E. Foulkes, S.J. Hill, Coupled techniques for arsenic speciation in food and drinking water: a review, J. Anal. Atom. Spectrom. 30 (2015) 102-118.

[20] M.R. Saidur, A.R.A. Aziz, W.J. Basirun, Recent advances in DNA-based electrochemical biosensors for heavy metal ion detection: A review, Biosens. Bioelectron. 90 (2017) 125-139.

[21] Y. Seok Kim, N.H. Ahmad Raston, M. Bock Gu, Aptamer-based nanobiosensors, Biosens. Bioelectron. 76 (2016) 2-19.

[22] R. Liu, Z. Chen, Y. Wang, Y. Cui, H. Zhu, P. Huang, W. Li, Y. Zhao, Y. Tao, X. Gao, Nanoprobes: quantitatively detecting the femtogram level of arsenite ions in live cells, ACS nano 5 (2011) 5560-5565.

[23] Y. Wu, S. Zhan, F. Wang, L. He, W. Zhi, P. Zhou, Cationic polymers and aptamers mediated aggregation of gold nanoparticles for the colorimetric detection of arsenic(III) in aqueous solution, Chem. Commun. 48 (2012) 4459-4461.

[24] R.P. Liang, Z.X. Wang, L. Zhang, J.D. Qiu, Label‐Free Colorimetric Detection of Arsenite Utilizing G‐/T‐Rich Oligonucleotides and Unmodified Au Nanoparticles, Chem.–Eur. J. 19 (2013) 5029-5033.

[25] M. Oroval, C. Coll, A. Bernardos, M.D. Marcos, R. Martínez-Máñez, D.G. Shchukin, F. Sancenón, Selective Fluorogenic Sensing of As(III) Using Aptamer-Capped Nanomaterials, ACS Appl. Mater. Inter. 9 (2017) 11332-11336.

[26] L. Zhang, X.-Z. Cheng, L. Kuang, A.-Z. Xu, R.-P. Liang, J.-D. Qiu, Simple and highly selective detection of arsenite based on the assembly-induced fluorescence enhancement of DNA quantum dots, Biosens. Bioelectron. 94 (2017) 701-706.

[27] Y. Wang, P. Wang, Y. Wang, X. He, K. Wang, Single strand DNA functionalized single wall carbon nanotubes as sensitive electrochemical labels for arsenite detection, Talanta 141 (2015) 122-127.

[28] L. Cui, J. Wu, H. Ju, Label-free signal-on aptasensor for sensitive electrochemical detection of arsenite, Biosens. Bioelectron. 79 (2016) 861-865.

[29] L. Gao, C. Lian, Y. Zhou, L. Yan, Q. Li, C. Zhang, L. Chen, K. Chen, Graphene oxide–DNA based sensors, Biosens. Bioelectron. 60 (2014) 22-29.

[30] Y. Wan, Y. Wang, J. Wu, D. Zhang, Graphene Oxide Sheet-Mediated Silver Enhancement for Application to Electrochemical Biosensors, Anal. Chem. 83 (2011) 648-653.

[31] Z. Chu, Y. Liu, W. Jin, Recent progress in Prussian blue films: Methods used to control regular nanostructures for electrochemical biosensing applications, Biosens. Bioelectron. 96 (2017) 17-25.

[32] J.-D. Qiu, H.-Z. Peng, R.-P. Liang, J. Li, X.-H. Xia, Synthesis, Characterization, and Immobilization of Prussian Blue-Modified Au Nanoparticles: Application to Electrocatalytic Reduction of H_2O_2, Langmuir 23 (2007) 2133-2137.

[33] J. Zhai, Y. Zhai, D. Wen, S. Dong, Prussian Blue/Multiwalled Carbon Nanotube Hybrids: Synthesis, Assembly and Electrochemical Behavior, Electroanal. 21 (2009) 2207-2212.

[34] G. Lai, H. Zhang, A. Yu, H. Ju, In situ deposition of Prussian blue on mesoporous carbon nanosphere for sensitive electrochemical immunoassay, Biosens. Bioelectron. 74 (2015) 660-665.

[35] E. Jin, X. Lu, L. Cui, D. Chao, C. Wang, Fabrication of graphene/prussian blue

composite nanosheets and their electrocatalytic reduction of H_2O_2, Electrochim. Acta 55 (2010) 7230-7234.

[36] X.-W. Liu, Z.-J. Yao, Y.-F. Wang, X.-W. Wei, Graphene oxide sheet–prussian blue nanocomposites: Green synthesis and their extraordinary electrochemical properties, Colloid. Surface. B 81 (2010) 508-512.

[37] R. Chen, Q. Zhang, Y. Gu, L. Tang, C. Li, Z. Zhang, One-pot green synthesis of Prussian blue nanocubes decorated reduced graphene oxide using mushroom extract for efficient 4-nitrophenol reduction, Anal. Chim. Acta 853 (2015) 579-587.

[38] J.-M. Bai, L. Zhang, R.-P. Liang, J.-D. Qiu, Graphene Quantum Dots Combined with Europium Ions as Photoluminescent Probes for Phosphate Sensing, Chem.–Eur. J. 19 (2013) 3822-3826.

[39] W. Li, Y. Yinjian, Z. Haozhi, S. Yonghai, H. Shuijian, X. Fugang, H. Haoqing, Controllable growth of Prussian blue nanostructures on carboxylic group-functionalized carbon nanofibers and its application for glucose biosensing, Nanotechnology 23 (2012) 455502.

[40] J.-L. Chen, X.-P. Yan, K. Meng, S.-F. Wang, Graphene Oxide Based Photoinduced Charge Transfer Label-Free Near-Infrared Fluorescent Biosensor for Dopamine, Anal. Chem. 83 (2011) 8787-8793.

[41] T. Uemura, S. Kitagawa, Prussian Blue Nanoparticles Protected by Poly(vinylpyrrolidone), J. Am. Chem.Soc. 125 (2003) 7814-7815.

[42] G.H. Clever, C. Kaul, T. Carell, DNA–Metal Base Pairs, Angew. Chem. Int. Edit. 46 (2007) 6226-6236.

[43] L. Zhang, Z.-X. Wang, R.-P. Liang, J.-D. Qiu, Easy Design of Colorimetric Logic Gates Based on Nonnatural Base Pairing and Controlled Assembly of Gold Nanoparticles, Langmuir 29 (2013) 8929-8935.

Table 1. As(III) detection in different samples by this method and ICP-MS (n = 3).

Samples	Added (ppb)	Found (ppb)	Relative Recovery [a] (%)	RSD (%)	ICP-MS (ppb)	Related Error (%)
Tap water 1	0	—	—	—	—	—
Tap water 2	0.2	0.19	95	4.9	0.2	-5.0
Tap water 3	10	10.2	102	3.9	9.9	3.0
River water 1	0	—	—	—	—	—
River water 2	0.2	0.192	96	4.5	0.2	-4.0
River water 3	10	10.5	105	5.1	10.1	4.0
Lake water 1	0	0.16	—	4.6	—	—
Lake water 2	0.2	0.362	101	4.2	0.21	-3.8
Lake water 3	10	10.76	106	3.6	10.1	4.9

[a] Relative Recovery (%) = $[(c_{Found} - c_{Blank}) / c_{Added}] \times 100$.

Figure Captions

Scheme 1. Schematic illustrations of the electrochemical biosensor fabrication process and the generation of PB NPs on GO sheets used as an electrochemical label for As(III) detection.

Fig. 1. CD spectra of 1 μM $(GT)_{21}$-ssDNA probe in the (a) absence and (b) presence of 1000 ppb As(III).

Fig. 2. SEM images of (A) ssDNA/MCH/AuE and (B) GO/ssDNA/MCH/AuE incubated with PB precursor solution.

Fig. 3. (A) CV and (B) EIS of the different electrodes in PBS buffer containing 5 mM $[Fe(CN)_6]^{3-/4-}$: (a) AuE, (b) ssDNA/MCH/AuE, (c) ssDNA/MCH/AuE incubated with GO, and (d) ssDNA/MCH/AuE first reacted with 100 ppb As(III) and then incubated with GO.

Fig. 4. (A) CVs of various electrodes in PBS buffer: (a) AuE, (b) ssDNA/MCH/AuE, (c) GO/ssDNA/MCH/AuE, (d) GO/ssDNA/MCH/AuE incubated with PB precursor solution, (e) ssDNA/MCH/AuE incubated with PB precursor solution, (f) ssDNA/MCH/AuE first reacted with 200 ppb As(III), then treated with GO and finally incubated with PB precursor solution. (B) Anodic peak current of electrode (d), (e) and (f).

Fig. 5. (A) DPV response curves of the biosensor with different concentrations of As(III): 0, 0.1, 0.2, 0.5, 1, 2, 5, 10, 20, 50, 100, 200, 300, 400 and 500 ppb (from a to b) in PBS buffer. (B) The plot of the peak currents intensity (near ~0.11 V) with As(III) concentrations ranging from 0 to 500 ppb in PBS buffer. Inset: the corresponding calibration plot of the DPV responses versus the logarithm value on As(III) concentrations. The error bars designate the standard deviation of three replicate tests.

Fig. 6. Target specificity investigation of the proposed electrochemical biosensor using various ions at the same concentration of 100 ppb (I_0 and I were the peak currents of the biosensor in the absence and presence of target ions, respectively.). The error bars designate the standard deviation of three replicate tests.

Scheme 1

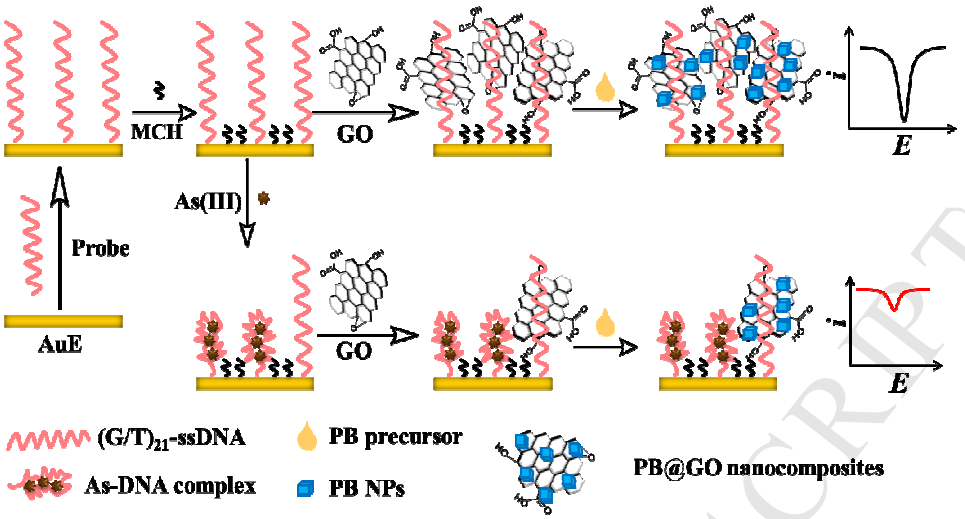

Fig. 1

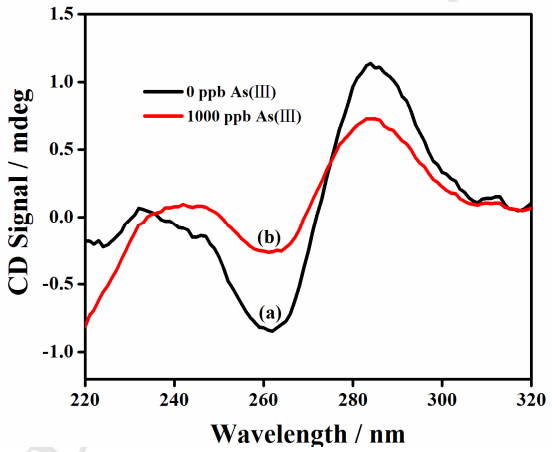

Fig. 2

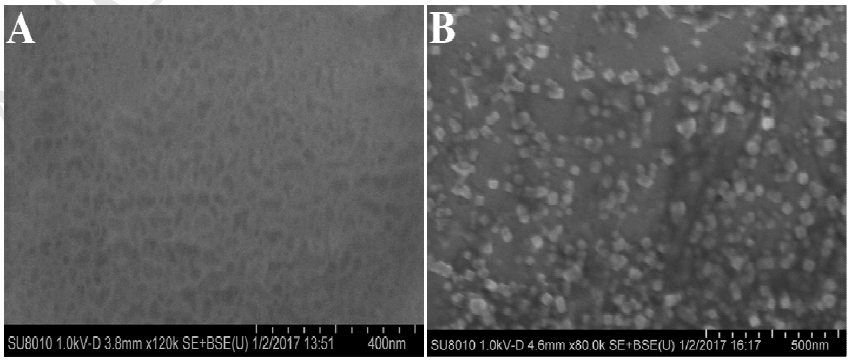

Fig. 3

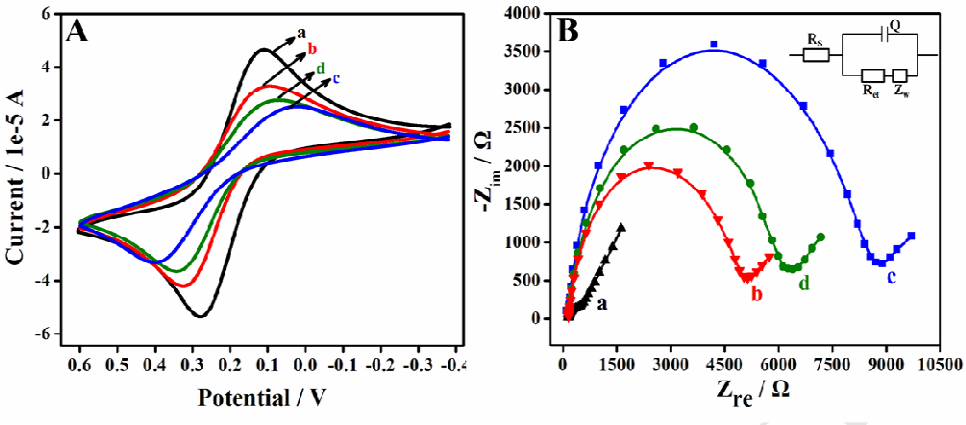

Fig. 4

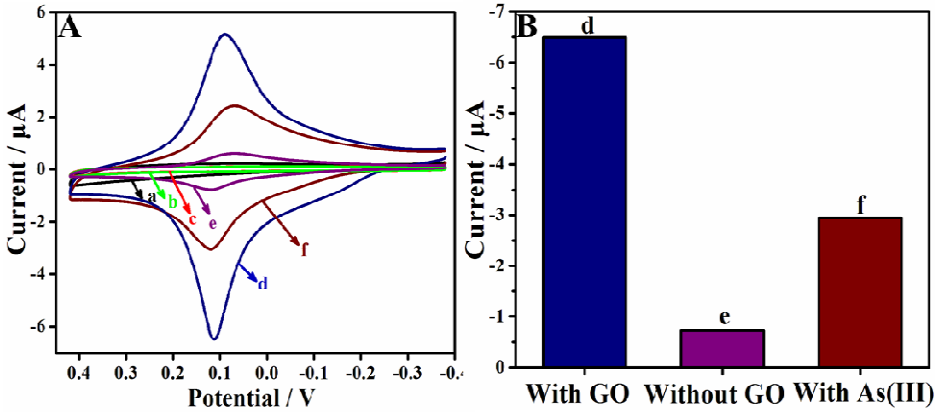

Fig. 5

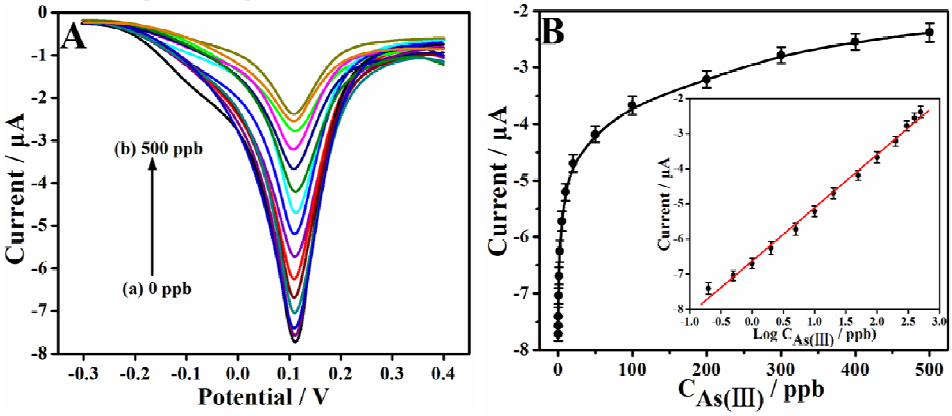

1 **Fig. 6**

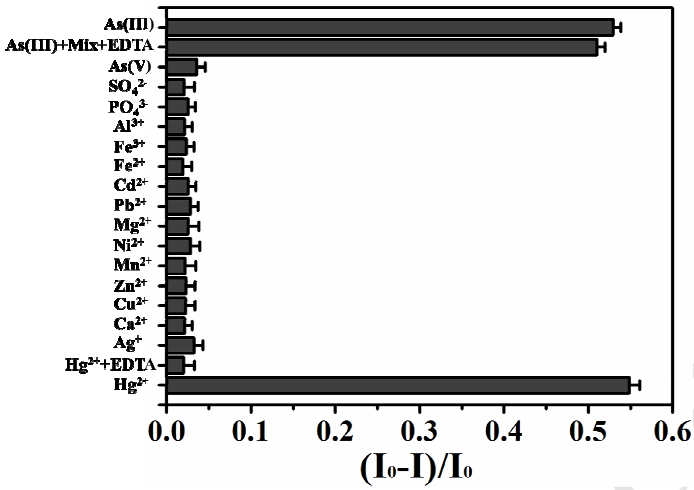

2

Highlights

- Graphene oxide was used as supporting matrix for the in-situ generation of PB NPs.
- Adsorption of GO on ssDNA can be regulated by As(III)-induced conformational change of $(GT)_{21}$-ssDNA.
- A sensor for As(III) detection was designed using GO-assisted generation of PB NPs as enhanced signal label.
- The sensor showed high sensitivity for As(III) with a detection limit of 0.058 ppb.
- The biosensor can be used for selective detection of As(III) in real water samples.